
Supplementary information

**Three-dimensional nanolithography
guided by DNA modular epitaxy**

In the format provided by the
authors and unedited

Three-dimensional nanolithography guided by DNA modular epitaxy

Jie Shen^{1,2}, Wei Sun^{1,2}, Di Liu^{1,2}, Thomas Schaus^{1,2} and Peng Yin^{1,2*}

¹ Wyss Institute for Biologically Inspired Engineering, Harvard University, Boston, Massachusetts 021152

² Department of Systems Biology, Harvard Medical School, Boston, Massachusetts 021151

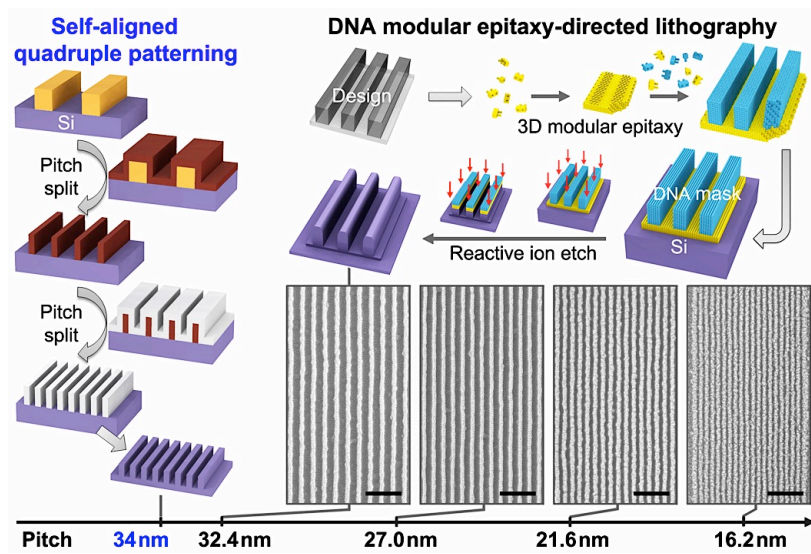
E-mail address: py@hms.harvard.edu

Supplementary Information

Contents

1. Summary figure	2
2. Supplementary methods	2
2.1. Cryo-electron microscopy	2
2.2. DNA mask deposition on silicon substrate	2
2.3. Atomic force microscopy	2
2.4. Scanning electron microscopy	3
2.5. Energy-dispersive X-ray mapping	3
2.6. Synthesis yield analysis	3
2.7. Pitch and critical dimension analysis	3
2.8. Roughness analysis	3
3. Supplementary figures	4
4. Supplementary tables	25

1 Summary figure



Summary Figure: Comparing with the quadruple patterning technique using repeated depositing and etching, DNA modular epitaxy-directed lithography encodes the designer patterns into self-assembled 3D DNA masks, and then uses single-run RIE to fabricate Si patterns at pitch sizes as small as 16.2 nm. All scale bars in the SEM images are 100 nm.

2 Supplementary methods

2.1. Cryo-electron microscopy

For cryo-EM sample preparation, 3 μL buffer solution of the DNA masks were deposited onto a glow-discharged C-flatTM holey carbon grid (CF-1.2/1.3-3C, *Electron Microscopy Sciences*) or copper grid (400 mesh) with a layer of ultrathin carbon film supported by a lacey carbon film (01824, *TED PELLA, INC.*). The solution was incubated on the EM grid for 30 min inside a humidity chamber. Then the EM grid was blotted for 4.0 s and immediately flash frozen by liquid nitrogen-cooled liquid ethane with a *CryoplungeTM 3* system (*Gatan, Inc.*). The EM grid was imaged in an *FEI Tecnai ArcticaTM* Microscope (equipped with an autoloader) operated at an acceleration voltage of 200 kV with an *FEI Eagle 4K* CCD camera. Cryo-EM images were recorded at a magnification of 39,000 \times with the defocus ranging from ca. $-0.5 \mu\text{m}$ to $-2.0 \mu\text{m}$ and at the dose rate of 25 electrons/ $(\text{\AA}^2\text{s})$ for 1.0 s exposure.

2.2. DNA mask deposition on silicon substrate

DNA masks were dried on silicon substrate for SEM, AFM imaging and RIE processing. We prepared a 100-fold dilution of DNA masks in 10 mM MgCl_2 solution. Then we dripped 2 μL of the solution onto a glow-discharged silicon substrate (5 mm \times 5 mm), and incubated with NiCl_2 solution (2 μL , 100 mM) for 1h inside a humidity chamber. After deposition, the silicon substrate was rinsed sequentially in 70 %, 90 % and 99.5 % ethanol followed by air-drying. The silicon substrate with fully dried DNA masks were used for dry-mode AFM measurement or RIE processing directly. For SEM imaging, the DNA mask-deposited silicon substrate was sputtered with a 1 nm-thick layer of Pt/Pd (80/20) to avoid charging effect.

2.3. Atomic force microscopy

The AFM measurements were implemented on a *Veeco Multimode SPM* system with silicon nitride SNL probes (*Bruker*, triangle cantilever C-type, resonant frequency 55 kHz in air). The scanning step was smaller than 2 nm (for instance, 512 scan lines for a 1 $\mu\text{m} \times 1 \mu\text{m}$ field). The dry samples (fully dried DNA masks or silicon patterns) were measured in the tapping-in-air AFM mode. The hydrous DNA masks were measured in the tapping-in-liquid AFM

mode. The tapping-in-liquid mode AFM sample was prepared as follows. A 100-fold dilution of DNA masks in 0.5×TE, 10 mM MgCl₂ solution (10 μL) was dipped onto a freshly cleaved mica substrate. After an incubation of 2 min, 5 μL of 10 mM NiCl₂ solution was added to promote the deposition of DNA mask onto the mica. Then the DNA mask deposited mica was scanned with a liquid quartz cell.

2.4. Scanning electron microscopy

The DNA masks and silicon patterns for SEM imaging were coated with 1-nm thick of Pt/Pd layer in a sputtering system (*EMS 300T D Sputter Coater*, 80:20 Pt/Pd target, 40 pA). SEM images were acquired on a *Zeiss FESEM Ultra Plus* system under high vacuum at an operation voltage of 10 kV, through 15 μm aperture, using a backscattering detector.

2.5. Energy-dispersive X-ray mapping

Energy-dispersive X-ray (EDX) spectrometer on a *Zeiss Supra 55VP* SEM system was used to map the elemental compositions of DNA masks and silicon patterns. The EDX signal was collected under high vacuum at an operation voltage of 5 kV, through 20 μm aperture, with 30 min acquisition time.

2.6. Synthesis yield analysis

In DNA modular epitaxy, the as-synthesized DNA brick crystals spontaneously precipitated from the reaction buffer. We assumed that all precipitated ssDNA components have been assembled into DNA brick crystals, thus an overall gross synthesis yield could be estimated by subtract the proportion of remaining ssDNAs (in supernatant reaction buffer) from 100 %, as shown by the following equation:

$$\text{Yield} \approx 100 \% - n_{\text{sup}} / n_{\text{all}}$$

n_{sup} is the mole amount of supernatant ssDNAs, per *NanoDrop* measurements (*Thermo Fisher 2000/2000C*). n_{all} is the total mole amount of ssDNAs added to the reaction, obtained from the *IDT* product specifications.

2.7. Pitch and critical dimension analysis

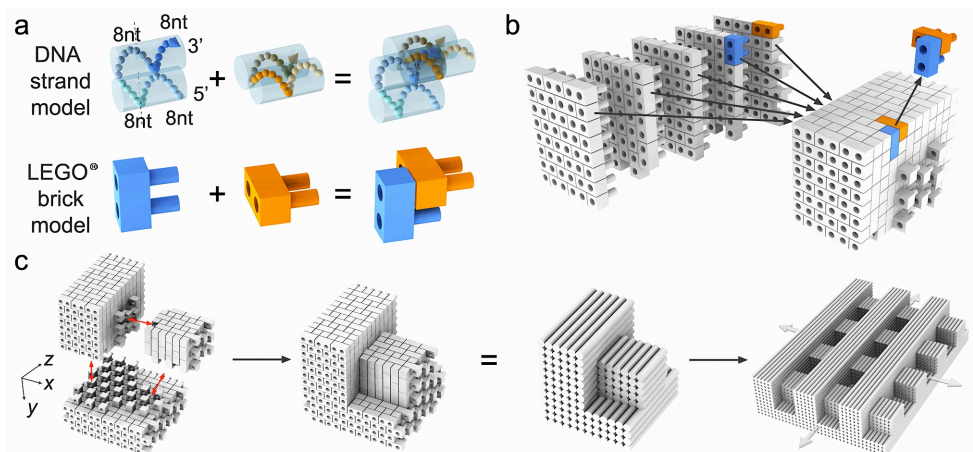
The critical dimensions (CDs, including widths and diameters of nanofeature) and pitches of DNA mask / silicon pattern were measured from SEM line-scan profiles. Taking the line/space DNA mask as an example, we first rotated the SEM beam scanning direction to the x axis of the targeting DNA mask, so as to get the SEM line-scan profiles that carrying the x - y cross-sectional information of the DNA mask. In subsequent data processing, we defined and measured the full width at half maximum (FWHM) of the SEM profile peaks as the line widths. The statistical mean value of the line width was defined as the CD.

On the same cross-sectional profile, we labeled the FWHM center point of each peak. The statistical mean distance of adjacent center points was defined as the full pitch (in the x axis) of this line/space mask. For each kind of sample, we randomly selected 20 independent DNA or silicon patterns to implement the statistical measurements.

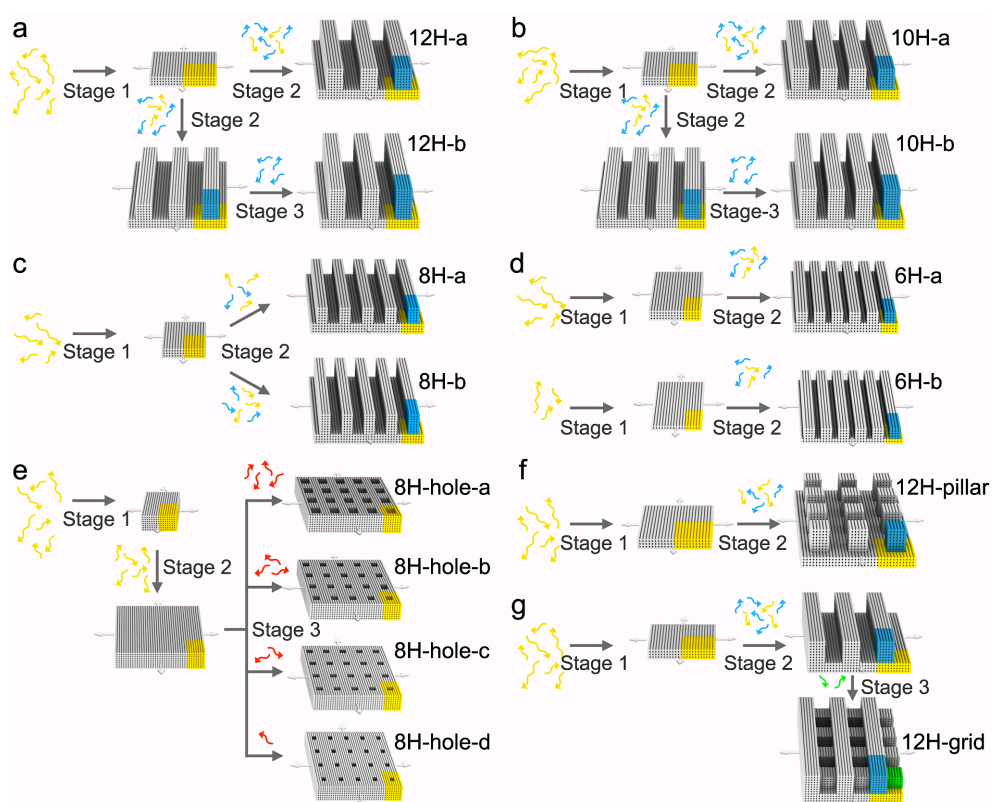
2.8. Roughness analysis

The surface roughness was calculated by AFM profiles (root mean square roughness). The line width roughness (LWR) was defined as three times of the line width standard deviation, basing on SEM measurements. For each kind of DNA mask or Si pattern, we selected a pattern area of 340 nm × 670 nm, and extracted 20 SEM profiles at an equal spacing to manually measure the line widths (i.e. FWHM of the SEM profiles).

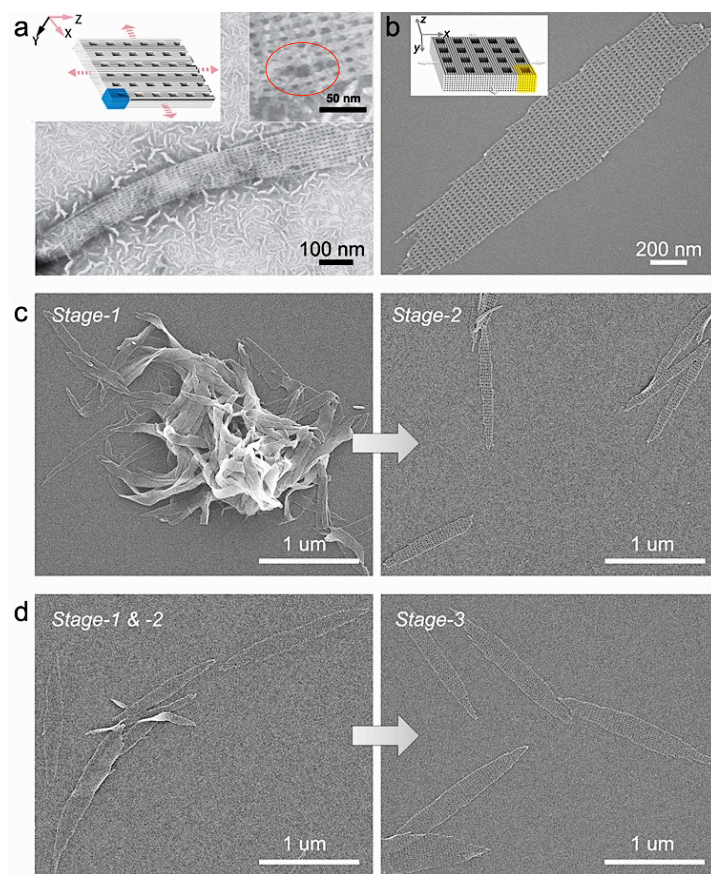
3. Supplementary figures



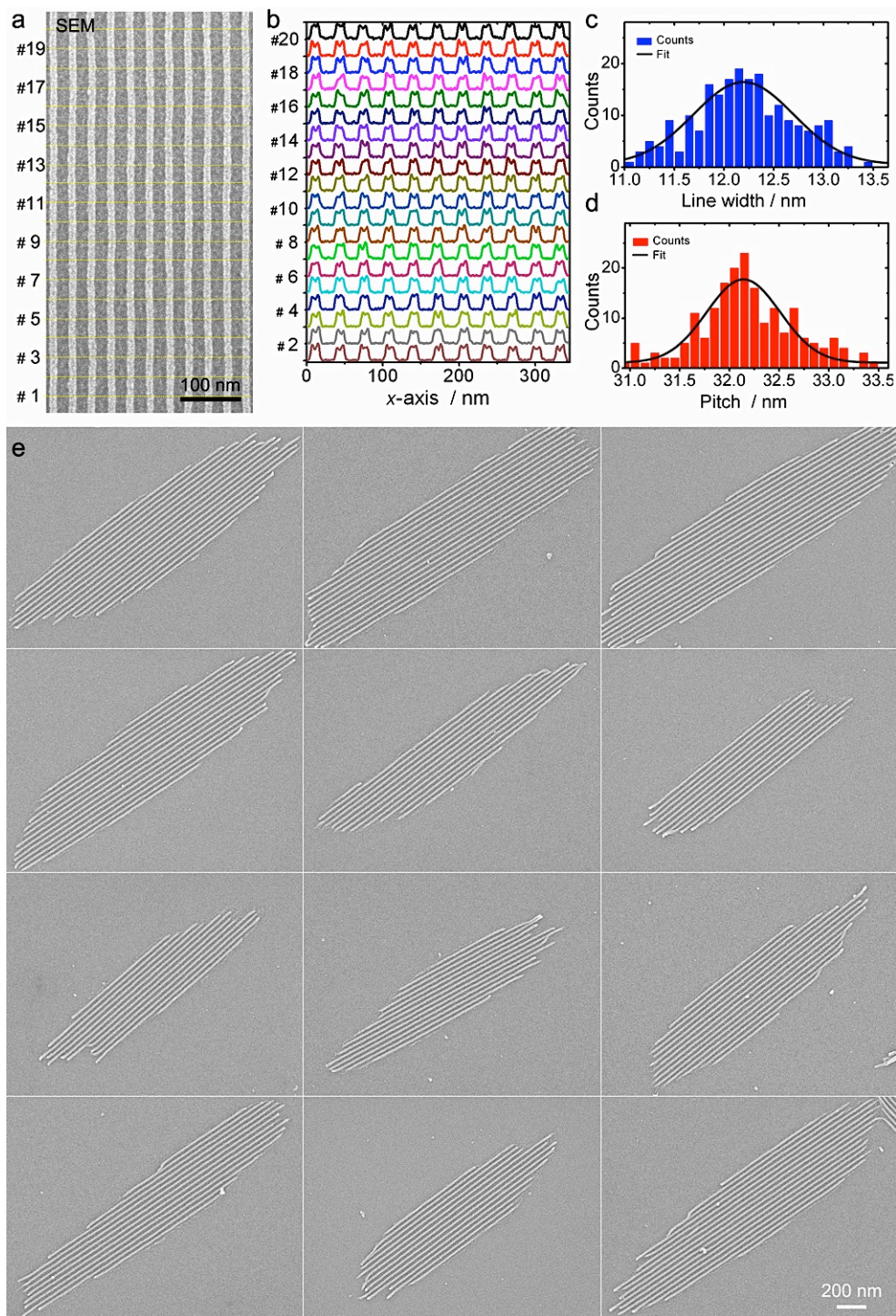
Supplementary Fig. 1 | Design of DNA brick crystal based 3D DNA mask. **a**, Schematic configurations of 32-nt DNA bricks in cylinder/strand model and LEGO model. Two neighboring DNA bricks hybridize their complementary 8-nt domains, forming a 90° dihedral angle. **b**, LEGO model of a 3D DNA module (6H × 8H × 94B) with sidewall connective DNA bricks. **c**, Combination of the taller-line module (6H × 8H × 94B), the lower-line module (6H × 5H × 47B) and the substrate module (12H × 4H × 94B) into a unit cell for an *x-z* extending DNA brick crystal. This *x-z* DNA brick crystal demonstrates a cross-line grid pattern with 32 nm pitch in both *x* and *z* axes.



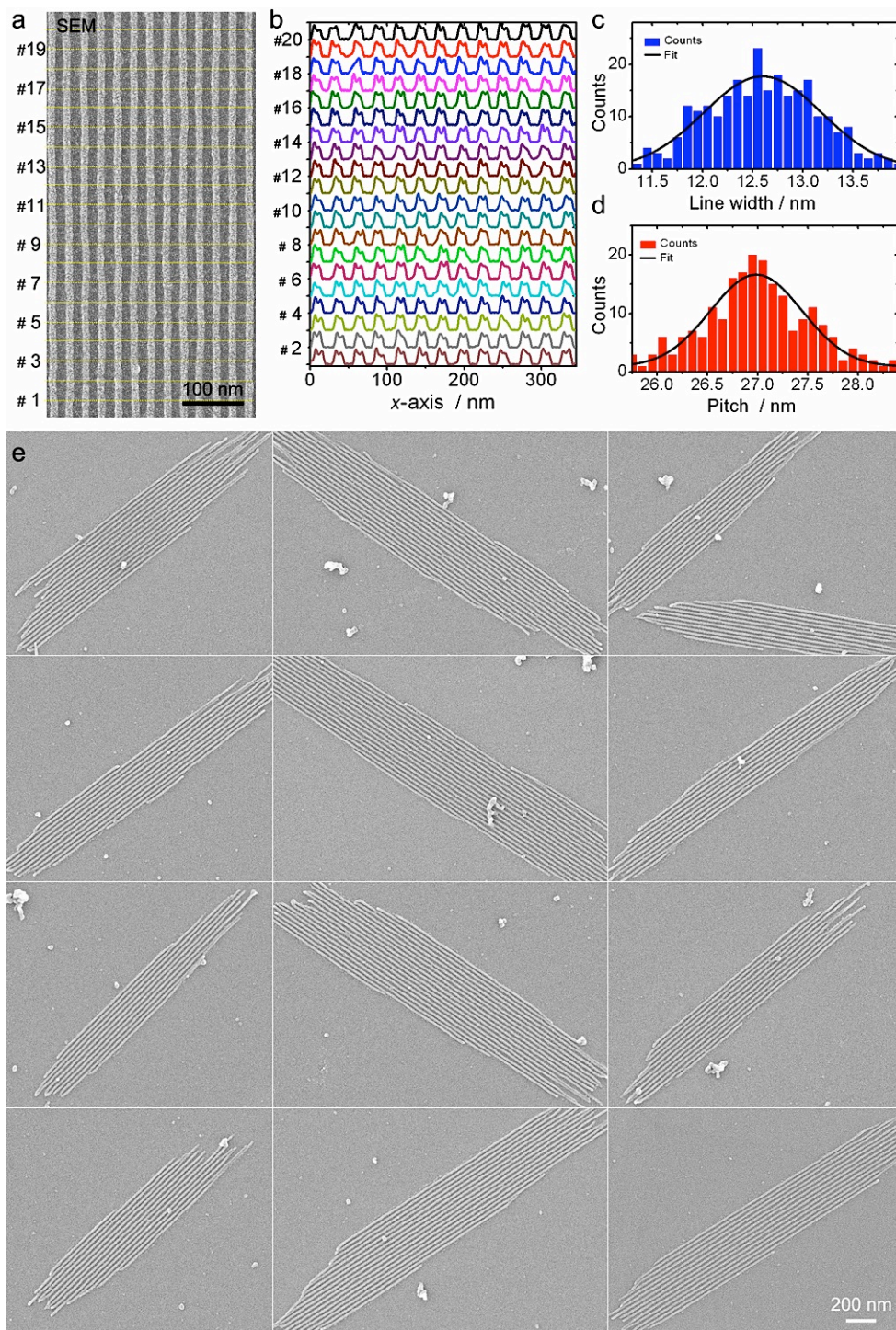
Supplementary Fig. 2 | DNA modular epitaxy flowchart. **a**, Line/space DNA mask at 32.4 nm pitch. **b**, Line/space DNA mask at 27.0 nm pitch. **c**, Line/space DNA mask at 21.6 nm. **d**, Line/space DNA mask at 16.2 nm. **e**, Contact hole DNA masks. **f**, Pillar array DNA mask. **g**, Cross-line grid DNA mask.



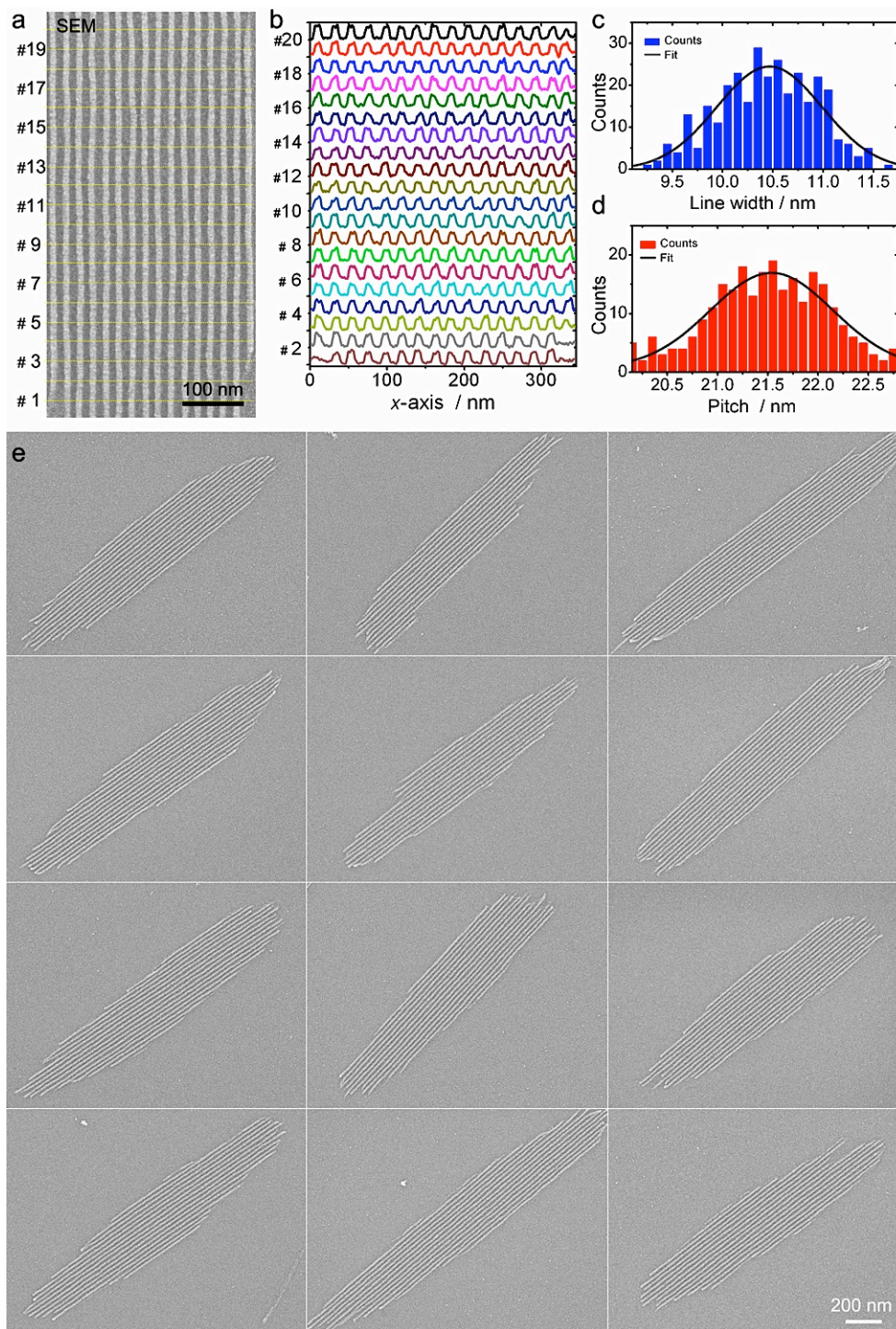
Supplementary Fig. 3 | DNA modular epitaxy and control study for contact hole DNA masks. **a**, TEM image of DNA brick crystal with contact hole feature of $2H \times 6H \times 32B$ along the x , y and z axes, assembled by one-pot annealing method following a 72 h linear cooling ramp from $60\text{ }^\circ\text{C}$ to $25\text{ }^\circ\text{C}$ (cited from Fig S19, *Nat. Chem.* **6**, 994–1002 (2014)). The inserted zoom-in image showed the grain boundary defects on hole sidewalls. **b**, SEM image of DNA brick crystal 8H-hole-a assembled by a three-stage DNA modular epitaxy. The x - z cross-section of the contact holes ($4H \times 47B$) in **b** is three times larger than that in **a** ($2H \times 32B$) but free-of grain boundary defects. **c**, left, SEM image of DNA substrates (module $8H \times 8H \times 94B$) for subtractive modular epitaxy, assembled from sub-optimal ssDNA concentrations (630 nM of each component ssDNA). The excessive seeding yield consumed too many ssDNAs so the subsequent epitaxial growth became insufficient. Right, SEM image of the corresponding subtractive modular epitaxial product. The average product size is $0.17 \pm 0.03\text{ }\mu\text{m} \times 1.1 \pm 0.3\text{ }\mu\text{m}$. **d**, left, SEM image of DNA substrates (module $8H \times 8H \times 94B$) assembled from optimal ssDNA concentrations (360 nM of each component ssDNA) by two-stages DNA module epitaxy. Right, SEM image of the corresponding subtractive modular epitaxy product. The average product size is $0.28 \pm 0.05\text{ }\mu\text{m} \times 1.8 \pm 0.4\text{ }\mu\text{m}$.



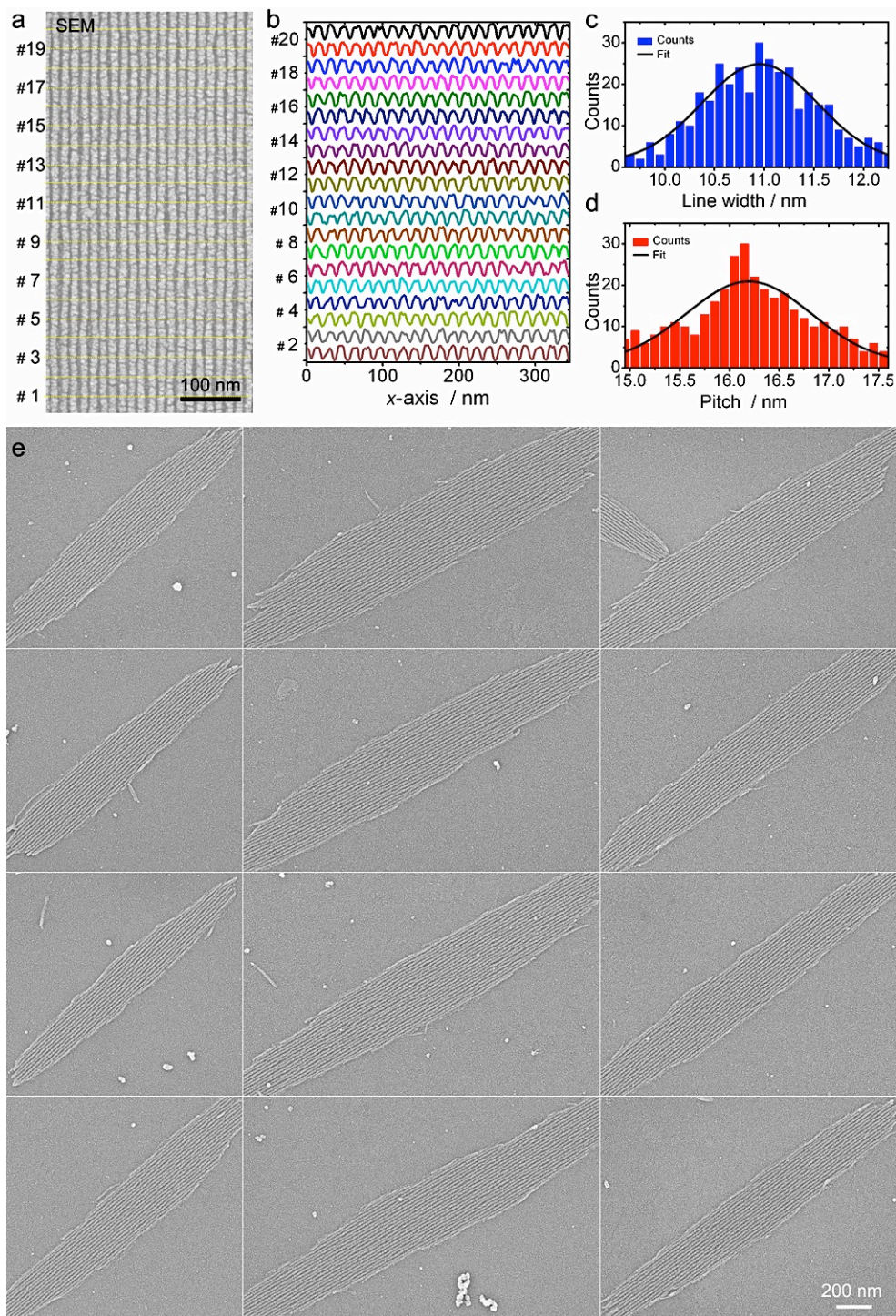
Supplementary Fig. 4 | Characterization of DNA mask 12H-a. **a**, SEM image section of DNA mask 12H-a with labeled scan-lines. **b**, The corresponding SEM line-scan profiles along the x axis. **c**, The histogram of DNA line width. **d**, The histogram of DNA line pitch. **e**, SEM images of randomly selected DNA mask 12H-a.



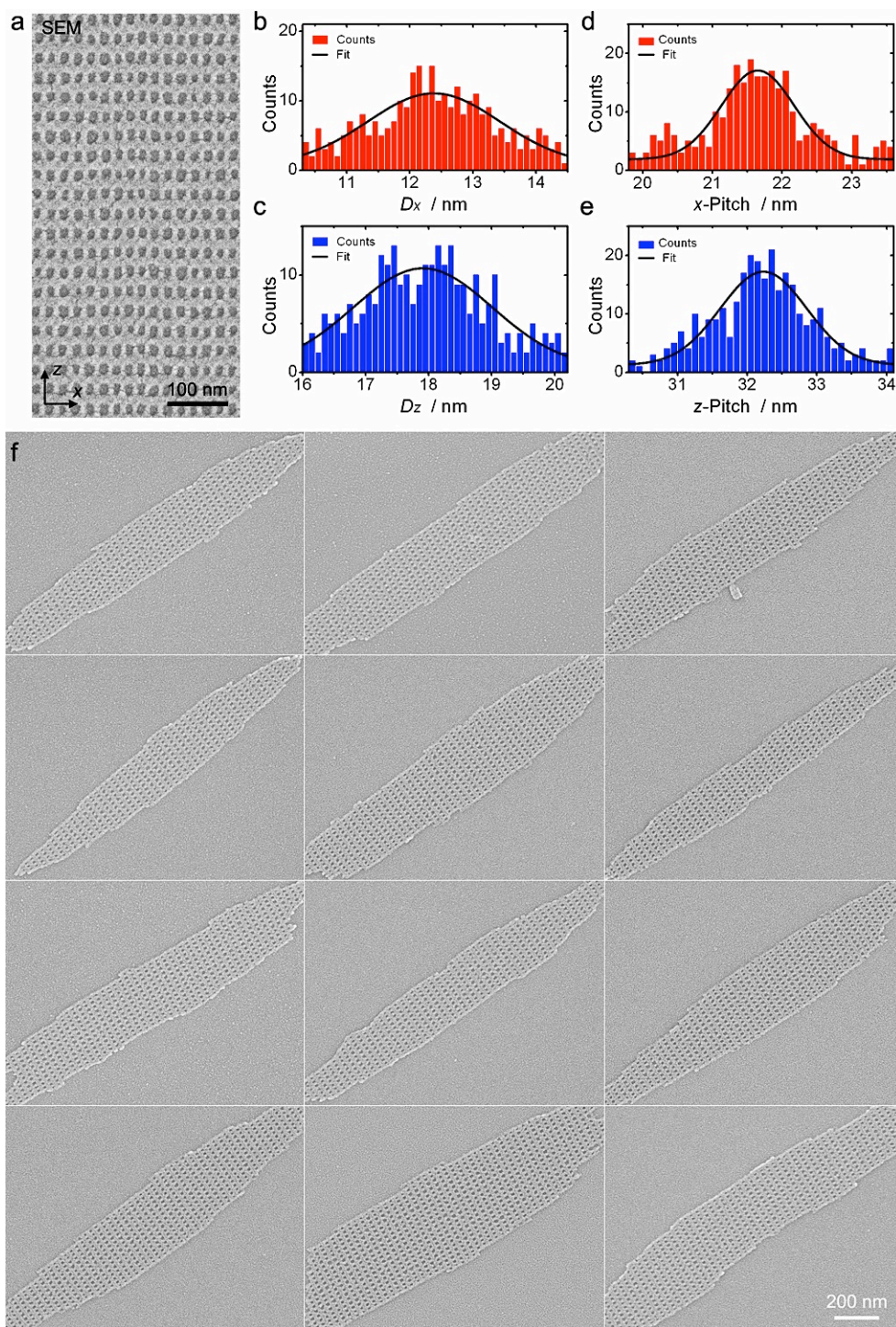
Supplementary Fig. 5 | Characterization of DNA mask 10H-a. **a**, SEM image section of DNA mask 10H-a with labeled scan-lines. **b**, The corresponding SEM line-scan profiles along the x axis. **c**, The histogram of DNA line width. **d**, The histogram of DNA line pitch. **e**, SEM images of randomly selected DNA mask 10H-a.



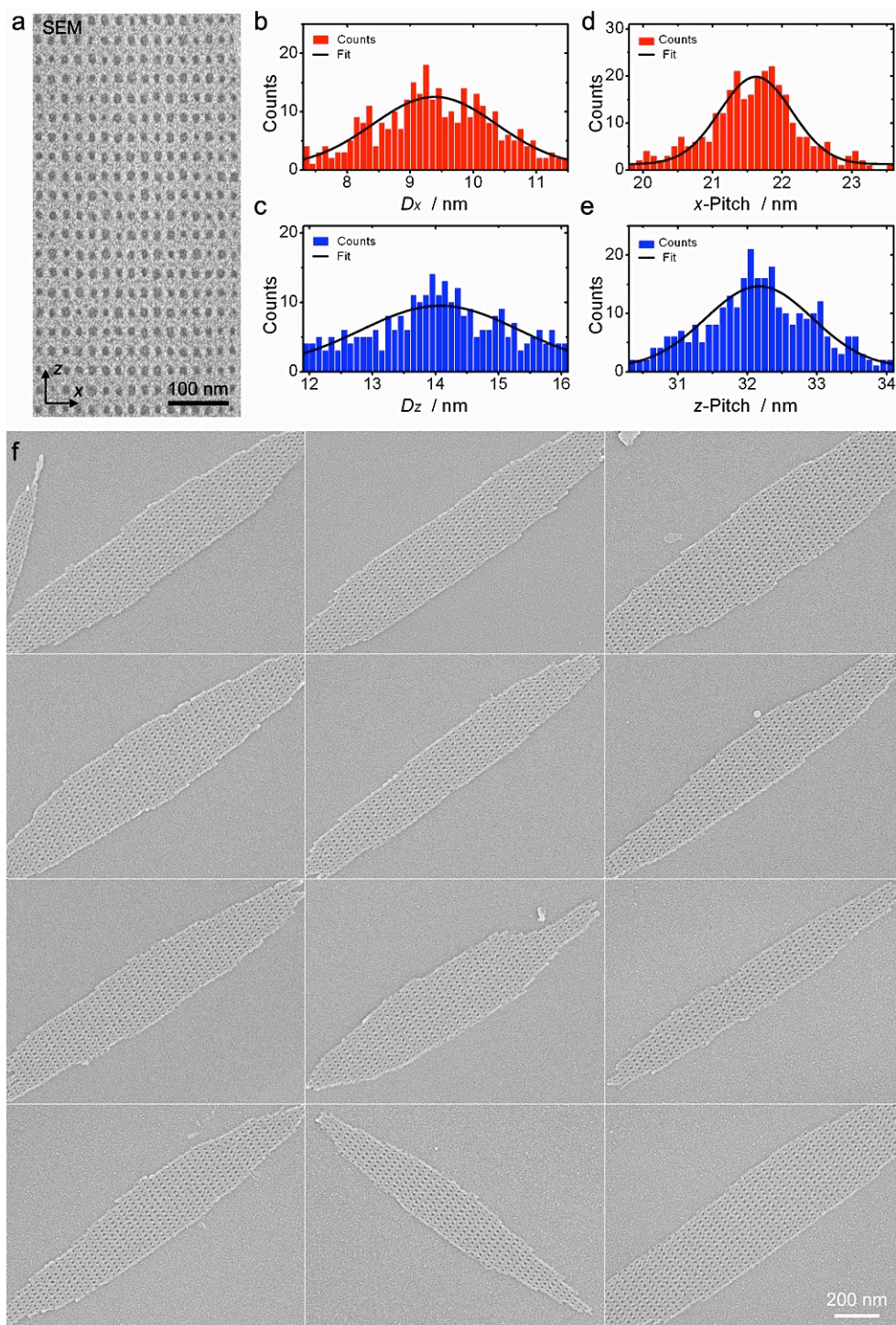
Supplementary Fig. 6 | Characterization of DNA mask 8H-a. **a**, SEM image section of DNA mask 8H-a with labeled scan-lines. **b**, The corresponding SEM line-scan profiles along the x axis. **c**, The histogram of DNA line width. **d**, The histogram of DNA line pitch. **e**, SEM images of randomly selected DNA mask 8H-a.



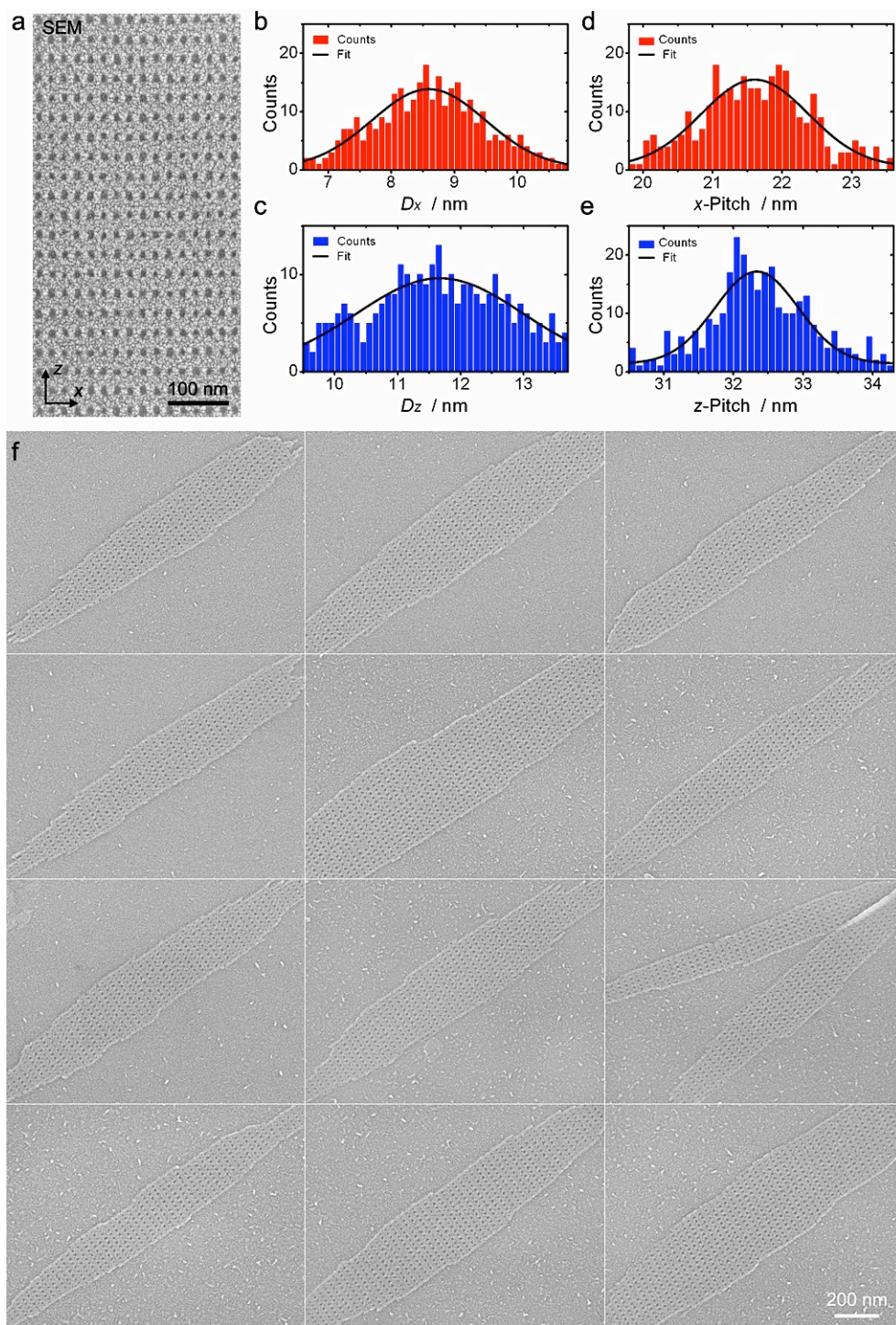
Supplementary Fig. 7 | Characterization of DNA mask 6H-a. **a**, SEM image section of DNA mask 6H-a with labeled scan-lines. **b**, The corresponding SEM line-scan profiles along the x axis. **c**, The histogram of DNA line width. **d**, The histogram of DNA line pitch. **e**, SEM images of randomly selected DNA mask 6H-a.



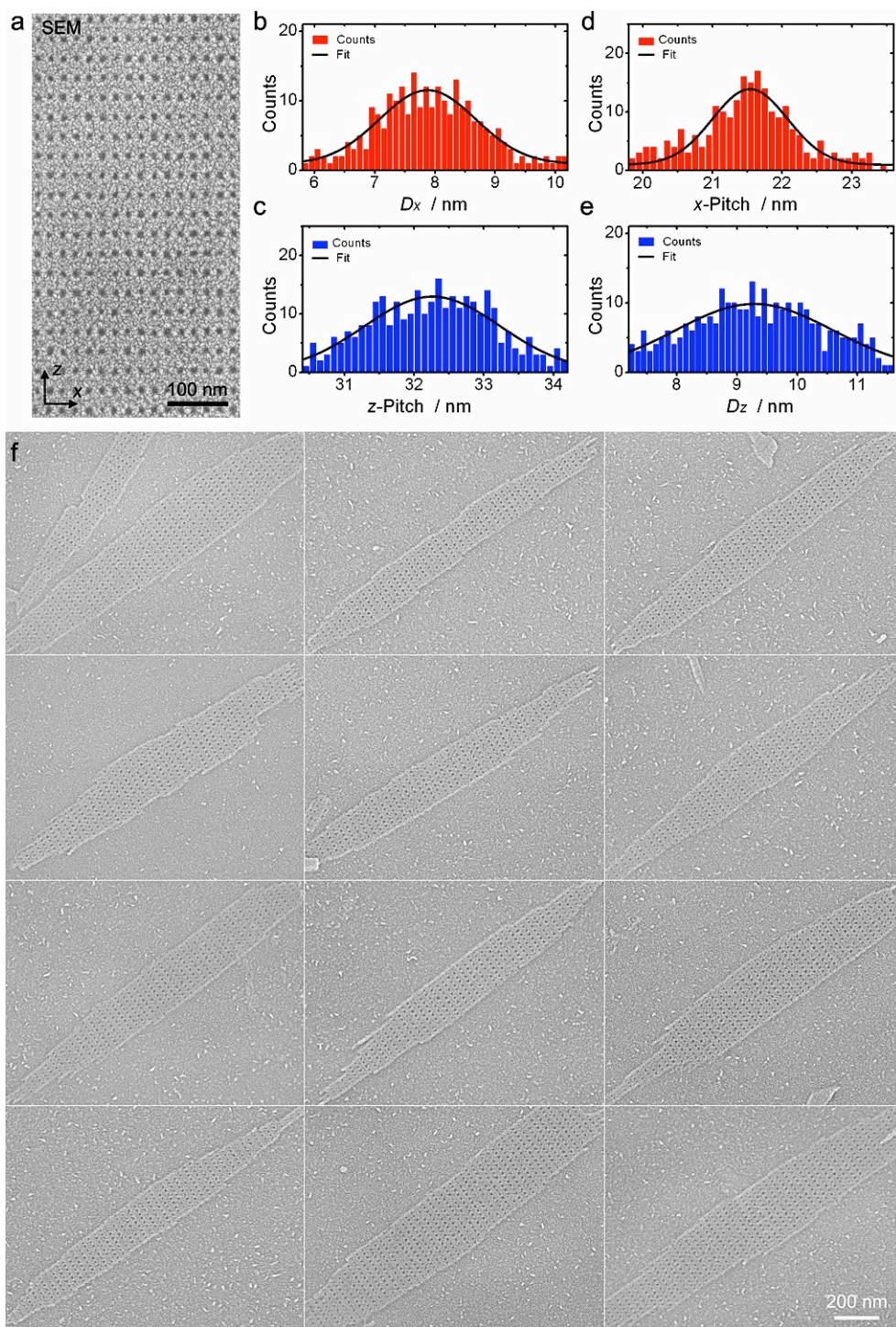
Supplementary Fig. 8 | Characterization of DNA mask 8H-hole-a. **a**, SEM image section of DNA mask. **b**, The histogram of hole diameter along the x axis (D_x). **c**, The histogram of hole diameter along the z axis (D_z). **d**, The histogram of hole pitch along the x axis. **e**, The histogram of hole pitch along the z axis. **f**, SEM images of randomly selected DNA mask 8H-hole-a.



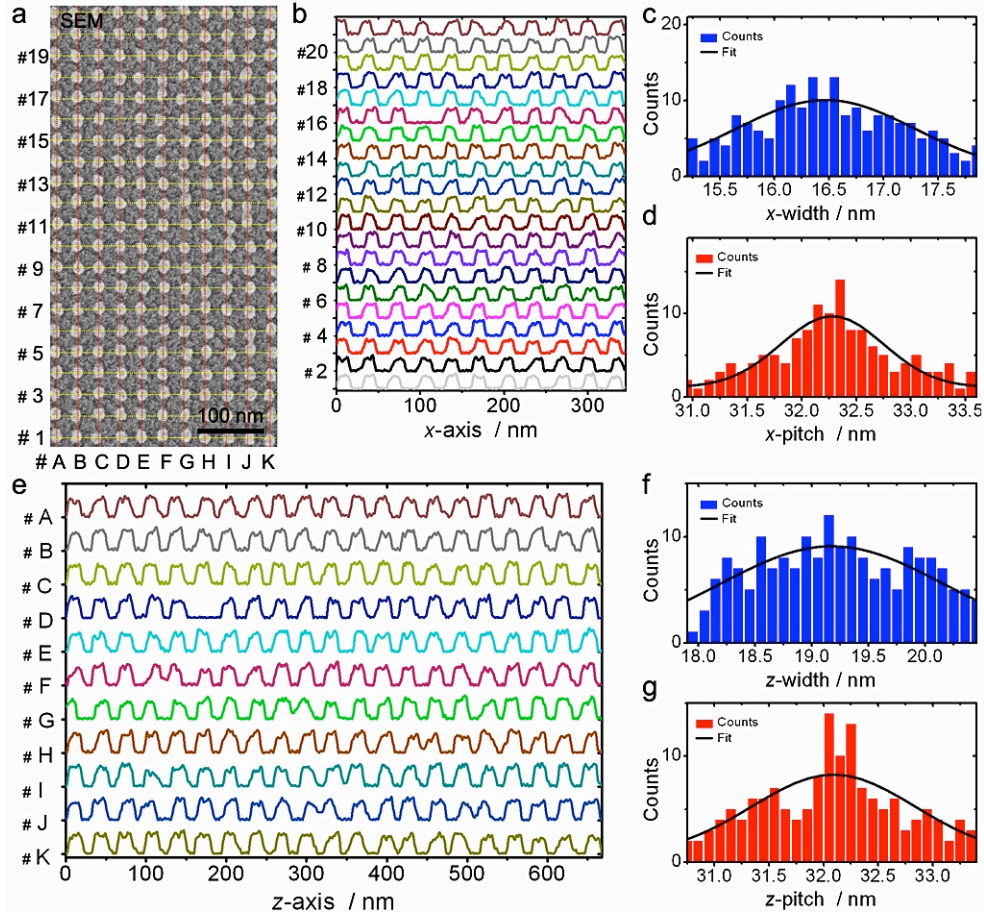
Supplementary Fig. 9 | Characterization of DNA mask 8H-hole-b. **a**, SEM image section of DNA mask. **b**, The histogram of hole diameter along the x axis (D_x). **c**, The histogram of hole diameter along the z axis (D_z). **d**, The histogram of hole pitch along the x axis. **e**, The histogram of hole pitch along the z axis. **f**, SEM images of randomly selected DNA mask 8H-hole-b.



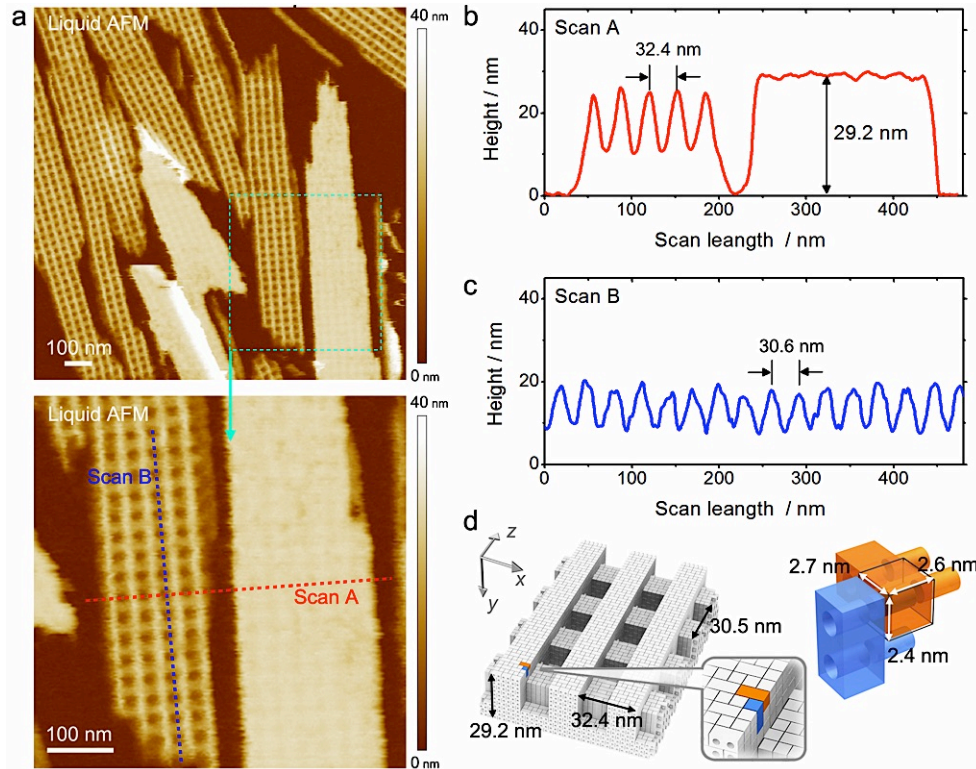
Supplementary Fig. 10 | Characterization of DNA mask 8H-hole-c. **a**, SEM image section of DNA mask. **b**, The histogram of hole diameter along the x axis (D_x). **c**, The histogram of hole diameter along the z axis (D_z). **d**, The histogram of hole pitch along the x axis. **e**, The histogram of hole pitch along the z axis. **f**, SEM images of randomly selected DNA mask 8H-hole-c.



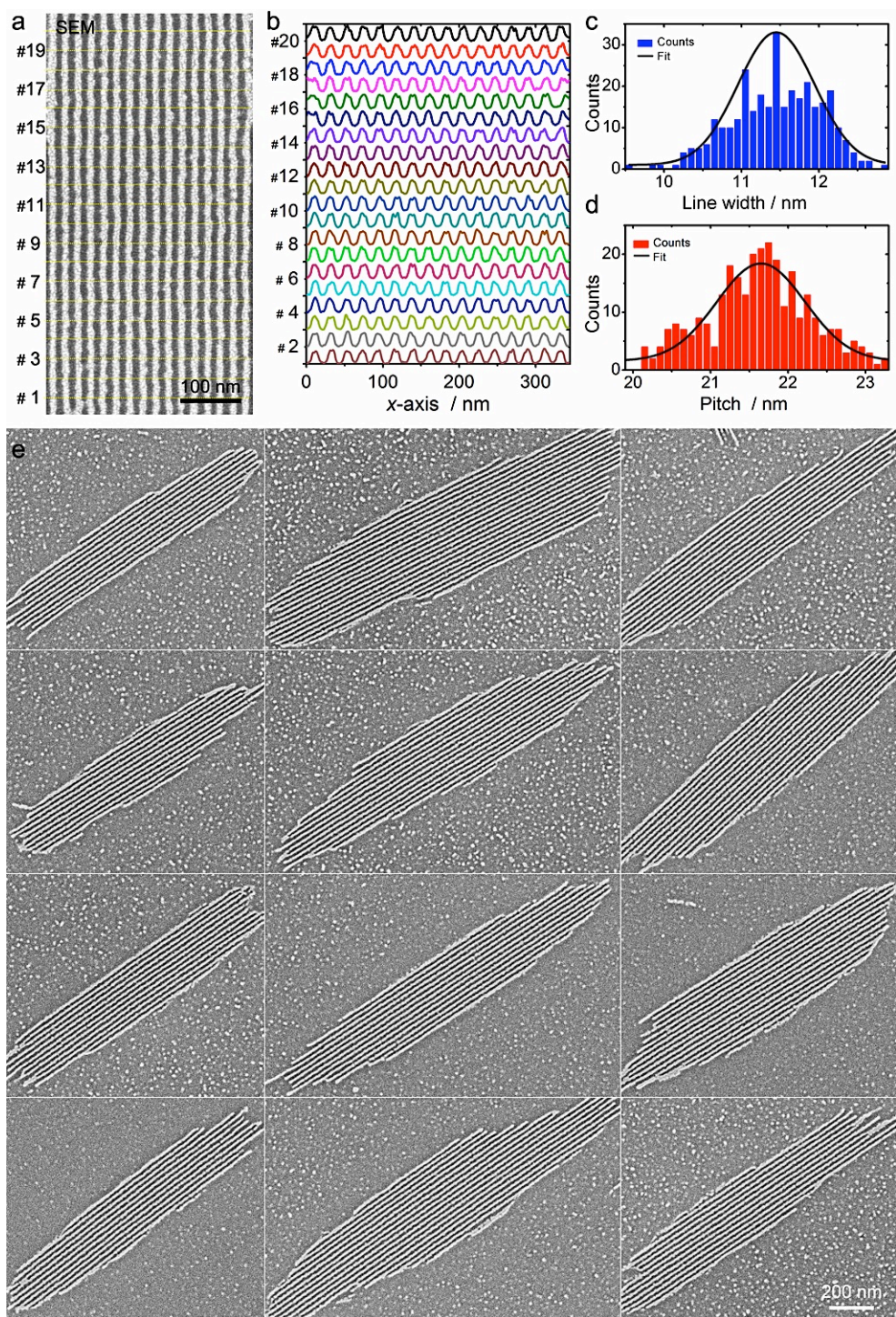
Supplementary Fig. 11 | Characterization of DNA mask 8H-hole-d. **a**, SEM image section of DNA mask. **b**, The histogram of hole diameter along the x axis (D_x). **c**, The histogram of hole diameter along the z axis (D_z). **d**, The histogram of hole pitch along the x axis. **e**, The histogram of hole pitch along the z axis. **f**, SEM images of randomly selected DNA mask 8H-hole-d.



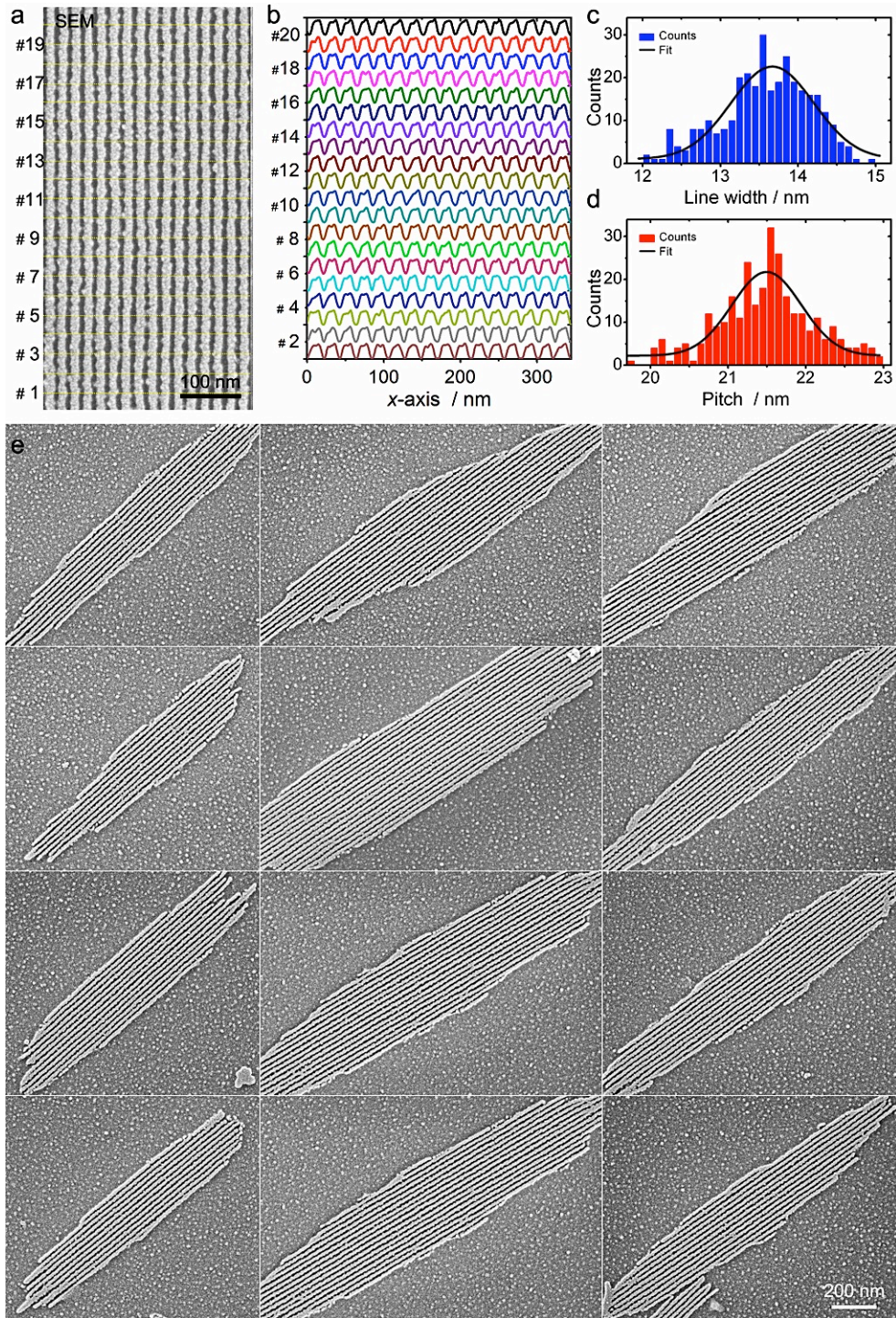
Supplementary Fig. 12 | Characterization of DNA mask 12H-pillar. **a**, SEM image section of DNA mask 12H-pillar with labeled scan-lines. **b**, The corresponding SEM line-scan profiles along the x axis. **c**, The histogram of pillar width long the x axis. **d**, The histogram of pitch long the x axis. **e**, The corresponding SEM line-scan profiles along the z axis. **f**, The histogram of pillar width long the z axis. **g**, The histogram of pitch long the z -axis.



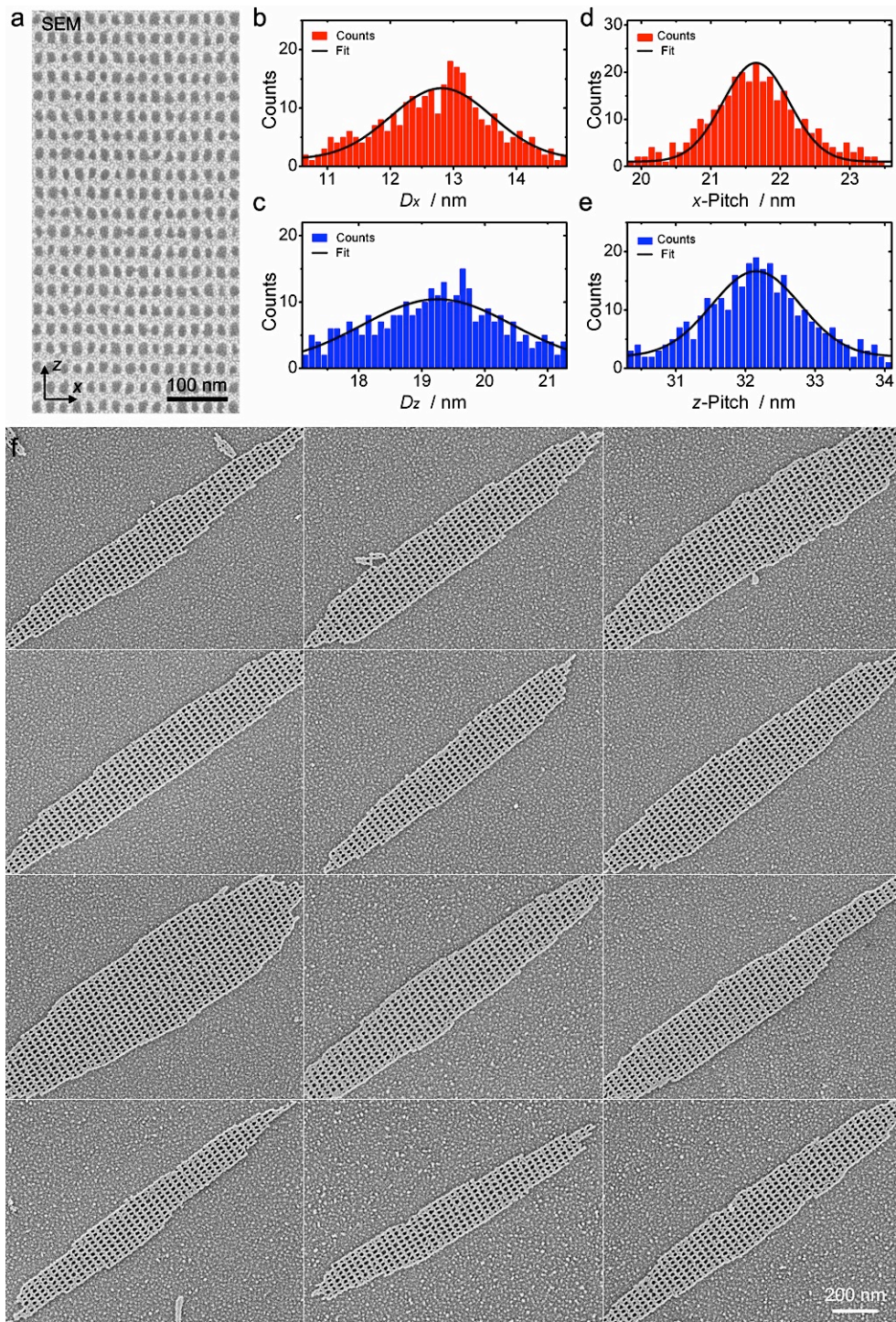
Supplementary Fig. 13 | Liquid-mode AFM measurement of DNA mask 12H-grid. **a**, The AFM images of hydrous DNA mask 12H-grid on mica. **b**, The AFM profile of the scan-line A (in red color) cuts DNA masks along the x axis. The AFM profile of the left-side DNA mask demonstrates a line pitch of 32.4 nm for the taller lines of 12H-grid. The AFM profile of the right-side DNA mask (upside-down deposited mask) indicates a vertical thickness of 29.2 nm for 12H-grid. The thickness difference between the face-up and upside-down DNA masks could be ascribed to the artifact from vertical pressure of AFM probe. **c**, The AFM profile of the scan-line B (in dark blue color) cuts DNA masks along the z axis. It demonstrates a line pitch of 30.6 nm for the lower lines of 12H-grid. **d**, Estimated dimensions of DNA brick voxel based on the liquid-mode AFM measurements. The approximate voxel dimensions are 2.7 nm \times 2.4 nm \times 2.6 nm along the x , y and z axes.



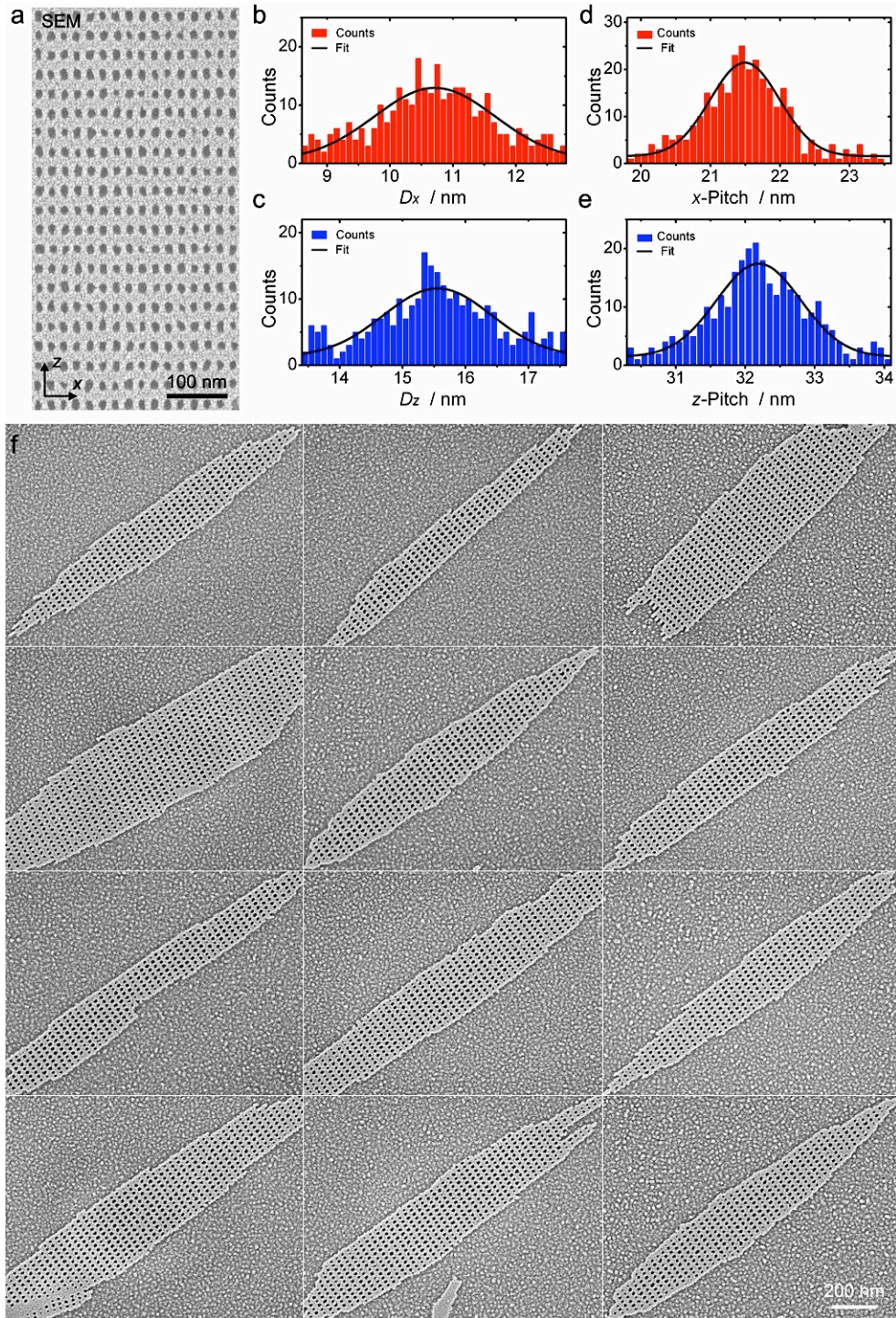
Supplementary Fig. 14 | Characterization of silicon pattern Si-8H-b-0H₂. **a**, SEM image section of silicon pattern Si-8H-b-0H₂ with labeled scan-lines. **b**, The corresponding SEM line-scan profiles along the x axis. **c**, The histogram of silicon line width. **d**, The histogram of silicon line pitch. **e**, SEM images of randomly selected silicon pattern Si-8H-b-0H₂.



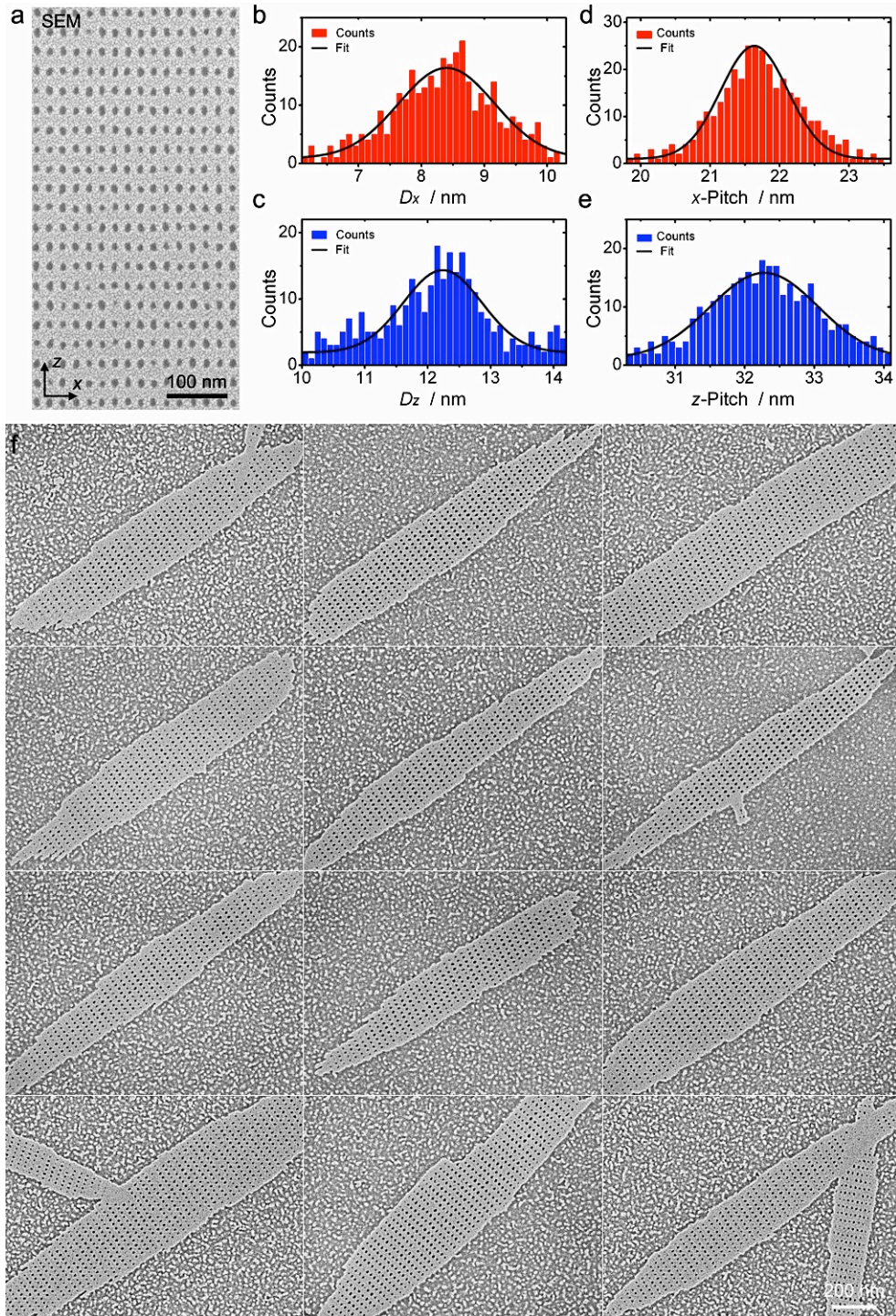
Supplementary Fig. 15 | **a**, SEM image section of silicon pattern Si-8H-b-1H₂ with labeled scan-lines. **b**, The corresponding SEM line-scan profiles along the x axis. **c**, The histogram of silicon line width. **d**, The histogram of silicon line pitch. **e**, SEM images of randomly selected silicon pattern Si-8H-b-1H₂.



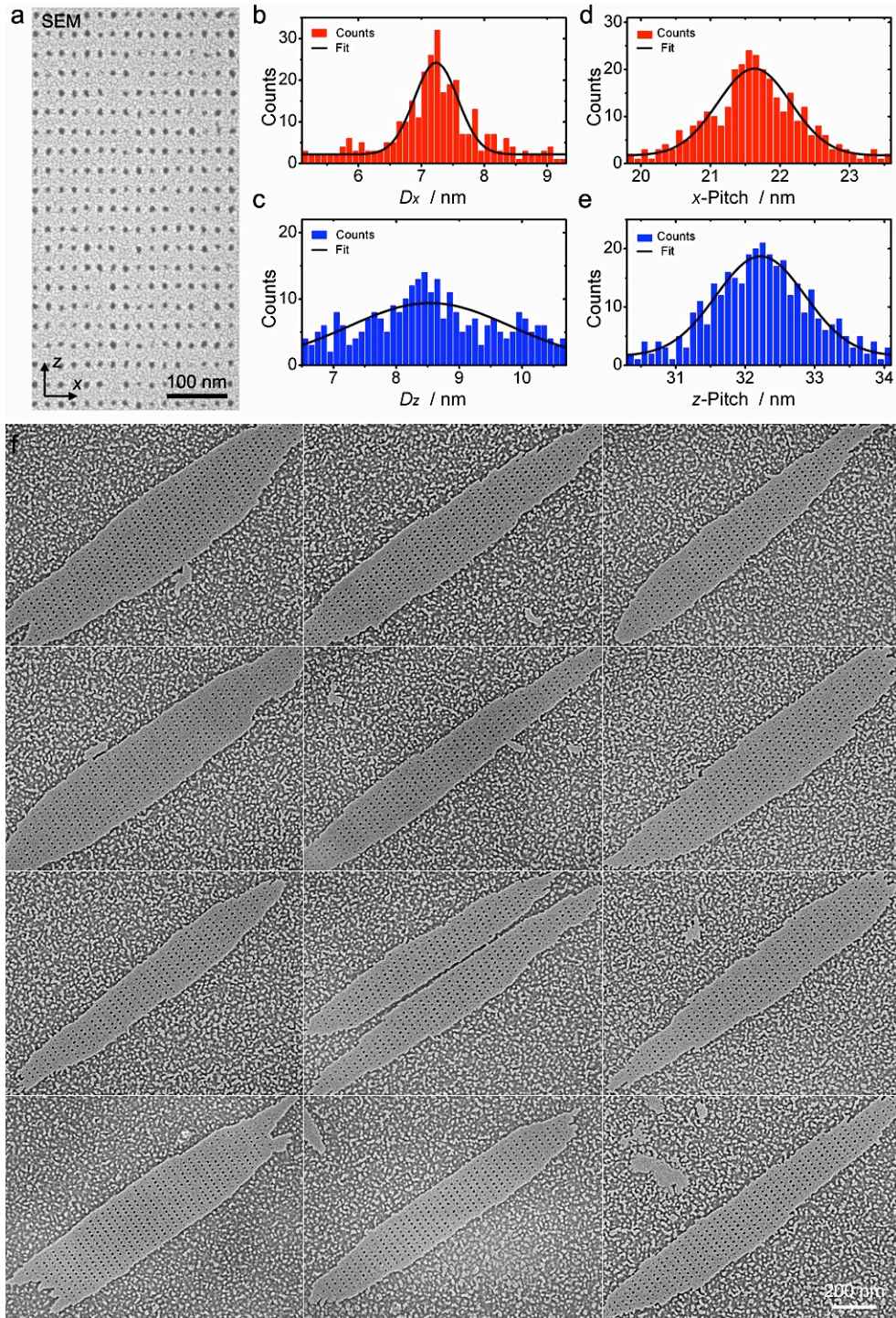
Supplementary Fig. 16 | Characterization of silicon pattern Si-8H-hole-a. **a**, SEM image section of silicon pattern Si-8H-hole-a. **b**, The histogram of hole diameter along the x axis (D_x). **c**, The histogram of hole diameter along the z axis (D_z). **d**, The histogram of hole pitch along the x axis. **e**, The histogram of hole pitch along the z axis. **f**, SEM images of randomly selected silicon pattern Si-8H-hole-a.



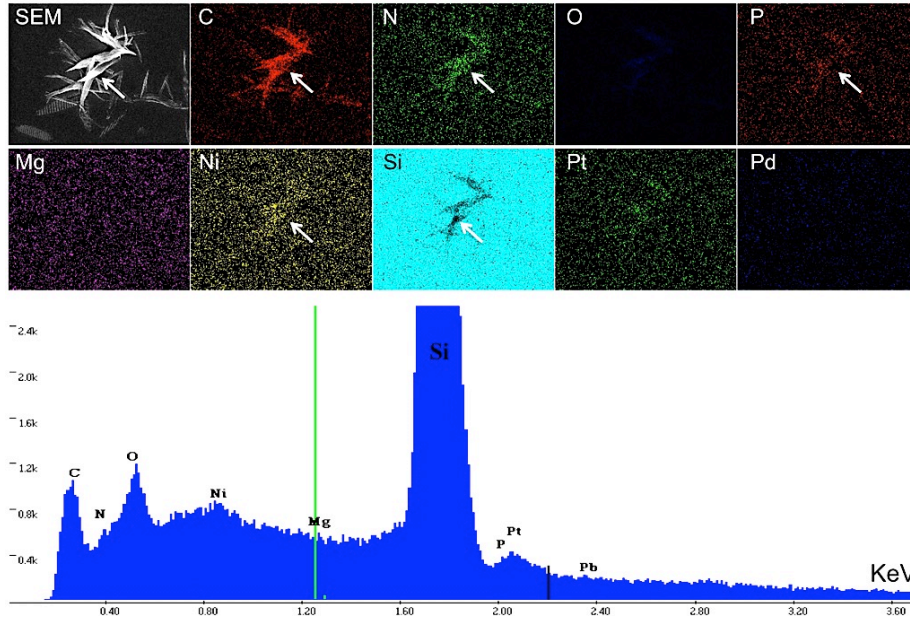
Supplementary Fig. 17 | Characterization of silicon pattern Si-8H-hole-b. **a** SEM image section of silicon pattern Si-8H-hole-b. **b**, The histogram of hole diameter along the x axis (D_x). **c**, The histogram of hole diameter along the z axis (D_z). **d**, The histogram of hole pitch along the x axis. **e**, The histogram of hole pitch along the z axis. **f**, SEM images of randomly selected silicon pattern Si-8H-hole-b.



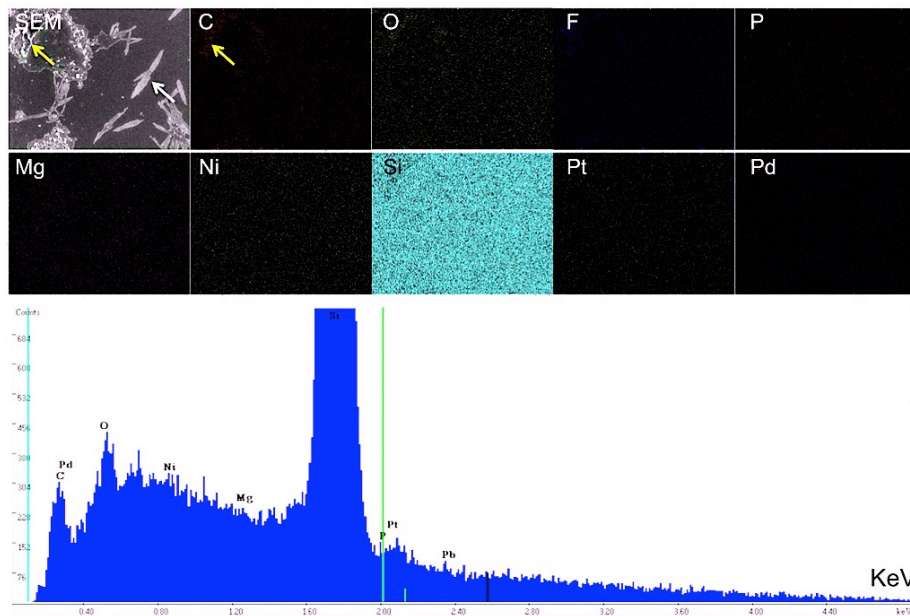
Supplementary Fig. 18 | Characterization of silicon pattern Si-8H-hole-c. a, SEM image section of silicon pattern Si-8H-hole-c.. b, The histogram of hole diameter along the x axis (D_x). c, The histogram of hole diameter along the z axis (D_z). d, The histogram of hole pitch along the x axis. e, The histogram of hole pitch along the z axis. f, SEM images of randomly selected silicon pattern Si-8H-hole-c.



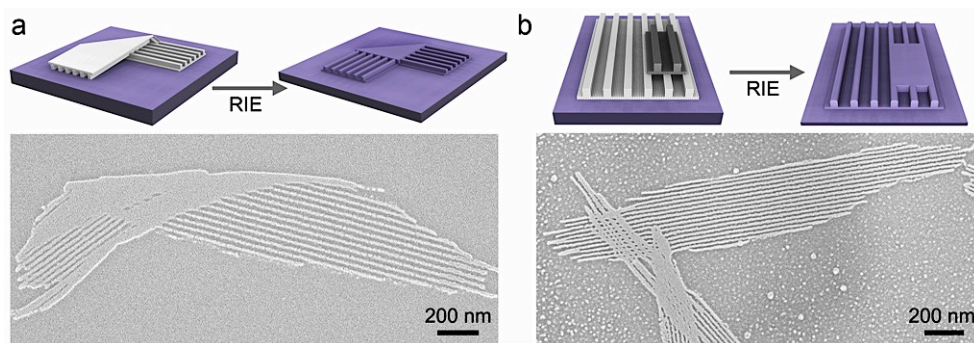
Supplementary Fig. 19 | Characterization of silicon pattern Si-8H-hole-d. **a**, SEM image section of silicon pattern Si-8H-hole-d. **b**, The histogram of hole diameter along the x axis (D_x). **c**, The histogram of hole diameter along the z axis (D_z). **d**, The histogram of hole pitch along the x axis. **e**, The histogram of hole pitch along the z axis. **f**, SEM images of randomly selected silicon pattern Si-8H-hole-d.



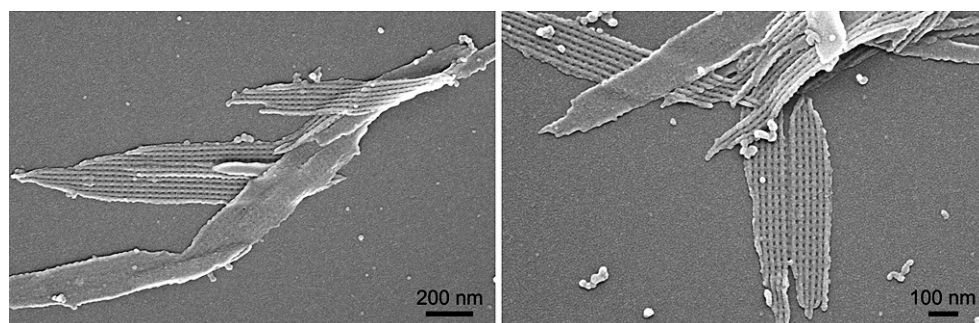
Supplementary Fig. 20 | EDX elemental map of DNA mask 12H-b. The arrowhead pointed to the DNA mask aggregates, where showed enhance EDX signals of carbon (C), nitrogen (N), phosphor (P) and nickel (Ni). EDX signal of silicon (Si) has been slightly blocked by the DNA mask aggregates. In the accumulated spectra, silicon contributed a majority of X-ray photon counts. The EDX signal of platinum (Pt) and palladium (Pd) came from the sputtering metal layer.



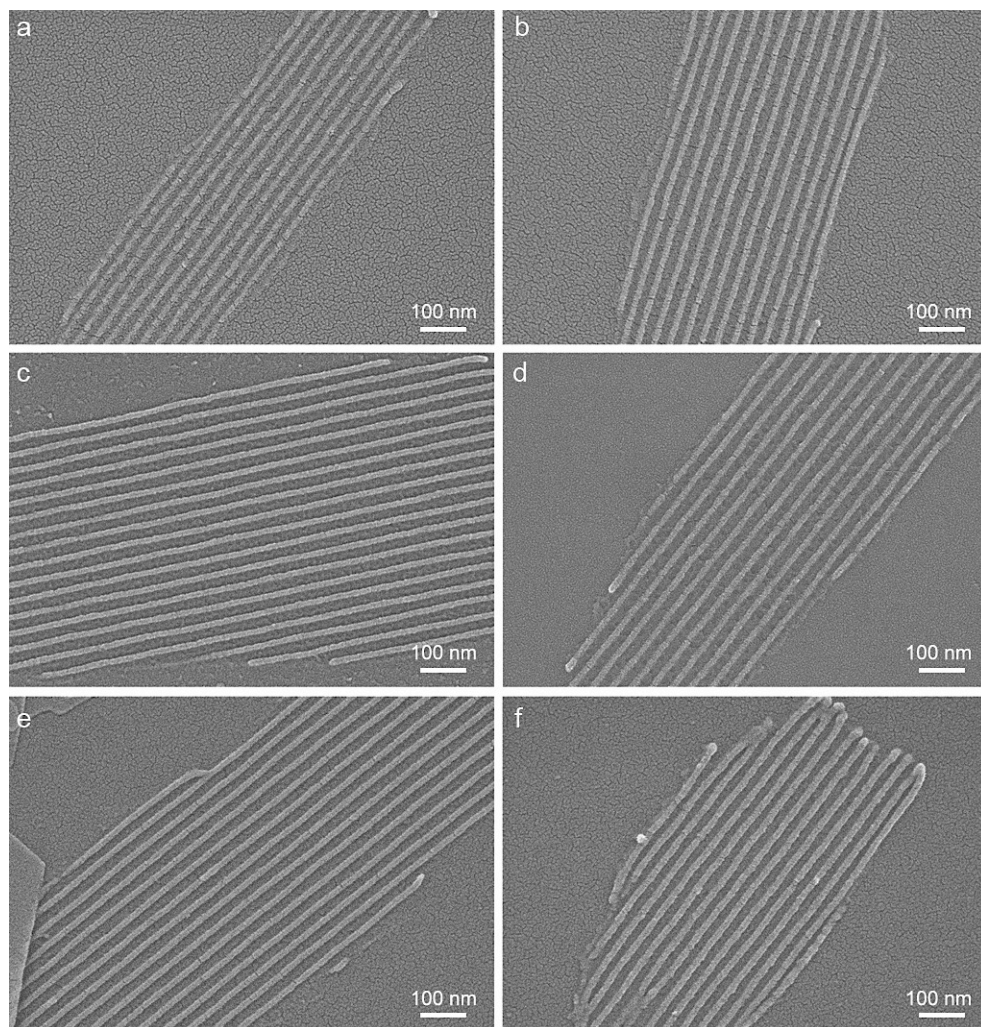
Supplementary Fig. 21 | EDX elemental map of silicon pattern Si-12H-b. The arrowhead pointed to fluorocarbon contaminations that still remained after hot piranha solution washing. The EDX map showed even distributions of silicon signal except in the fluorocarbon covered region. In the accumulated spectra, only trace amounts of oxygen (O), nickel (Ni), platinum (Pt) and palladium (Pd) could be found.



Supplementary Fig. 22 | RIE products from atypical deposited DNA masks. **a**, Scheme and SEM characterization of silicon pattern etched from a folded DNA mask 12H-a. The face-up part of DNA mask produced the right-side silicon lines with a regular line pitch at 32.4 nm. The overlapping region of DNA mask produced the middle silicon deck with a flat surface. The upside-down part of DNA mask produced the left-side silicon lines. The unrestricted DNA substrate could easily shrink under RIE heating effect, resulting in a decreased line pitch at 25.1 nm. **b**, Scheme and SEM characterization of silicon patterns etched from partially overlapped DNA masks 8H-b. The single layered DNA mask produced regular silicon lines at 21.6 nm pitch. The overlapped mask regions resulted in the silicon deck and the mesh structures.



Supplementary Fig. 23 | DNA Mask deposition without Ni^{2+} . SEM images of DNA mask 12H-grid deposited on a silicon substrate without Ni^{2+} treatment (only containing MgCl_2). The mask lines have partially collapsed in the drying process, leading to increased line widths and flattened 3D morphology comparing with the Ni^{2+} -treated samples. The Ni^{2+} -free DNA mask 12H-grid also showed variable shrinkage on its line pitches.



Supplementary Fig. 24 | DNA Mask deposition with different metal ions. SEM images of DNA mask 12H-a deposited on silicon substrates with (a) MgCl_2 only, (b) CoCl_2 , (c) NiCl_2 , (d) CuCl_2 , (b) ZnCl_2 , and (b) AlCl_3 .

4. Supplementary tables

Supplementary Table 1. Gross synthesis yield of DNA modular epitaxy

N is the amount of composing ssDNAs in a 3D DNA module design; c is the initial molar concentration of each ssDNA in the reaction mixture, calculated from the ssDNA concentration of *IDT* stock solutions and the pipetting stoichiometry; C is the molar concentration of all existing DNA in the reaction mixture (including the remaining ssDNAs and assembled DNA bricks), equal to $\sum c \cdot N$; ρ' is the mass concentration of all remaining ssDNAs in the reaction mixture, measured by *NanoDrop*; C' is the molar concentration of remaining ssDNAs that calculated from ρ' , according to an average molecular weight (M_w) of 327 for deoxyribonucleotide monophosphate; c' is the molar concentration of each remaining ssDNA, equal to C'/N ; GY is the gross synthesis yield, equal to $100\% - C'/C$.

Epitaxial Stage-1

	N_{sub}	c_{sub} nmol/L	C_{sub} nmol/L	ρ_1' ng/uL	C_1' nmol/L	c_1' nmol/L	GY_1
12H-a/b	288	313	90,000	150	14,275	49.6	84.1 %
10H-a/b	240	375	90,000	76	7,188	30.0	92.0 %
8H-a/b	192	469	90,000	115.9	11,029	57.4	87.7 %
6H-a	144	313	45,000	145	13,658	94.8	69.6%
6H-b	72	313	22,500	49	4,434	61.6	80.3 %
8H-hole	384	350	134,000	385	37,807	98.5	71.8 %
12H-Pillar	288	313	90,000	143	13,750	47.7	84.7 %
12H-Grid	288	313	90,000	153	14,266	49.5	84.1 %

Epitaxial Stage-2

	N_{top}	c_{top} nmol/L	$C_{\text{sub+top}}$ nmol/L	ρ_2' ng/uL	C_2' nmol/L	c_2' nmol/L	GY_2
12H-a	312	230	125,580	156	16,596	30.4	86.7 %
12H-b	234	216	134,784	186	19,787	31.7	85.3 %
10H-a	312	266	131,404	168	17,872	36.2	86.4 %
10H-b	234	247	141,284	286	30,426	53.2	78.5 %
8H-a	162	243	89,910	129	13,950	37.7	84.5 %
8H-b	216	209	88,616	118	12,795	30.2	85.6 %
6H-a	108	217	57,288	92	9,938	37.6	82.6 %
6H-b	108	256	72,192	49	8,077	28.6	88.8 %
8H-hole	408	266	106,400	285	29,153	72.9	72.6 %
12H-Pillar	159	192	90,432	165	17,666	37.5	80.5 %
12H-Grid	319	214	135,034	345	37,114	58.8	72.5 %

Epitaxial Stage-3

	N_{top2}	c_{top2} nmol/L	$C_{\text{sub+top}}$ nmol/L	ρ_3' ng/uL	C_3' nmol/L	c_3' nmol/L	GY_3
12H-b	234	192	149,760	232	24,681	31.6	83.5 %
10H-b	234	214	155,792	299	31,809	43.7	79.6 %
Grid	78	181	128,329	181	18,922	26.7	85.3 %

Supplementary Table 2. AFM/SEM measurement results of 3D DNA masks.

DNA masks	Defects rate	x-axis pitch	z-axis pitch	Thickness	Critical dimension
12H-a	0 per μm^2	32.2 ± 0.6 nm	N/A	18.5 ± 0.6 nm	<i>WD</i> 12.2 ± 0.5 nm
12H-b	0 per μm^2	32.3 ± 0.6 nm	N/A	24.4 ± 0.7 nm	<i>WD</i> 14.9 ± 0.4 nm
10H-a	0.1 per μm^2	27.0 ± 0.8 nm	N/A	19.5 ± 0.8 nm	<i>WD</i> 12.6 ± 0.6 nm
10H-b	0.2 per μm^2	27.0 ± 0.8 nm	N/A	24.2 ± 0.5 nm	<i>WD</i> 14.0 ± 0.5 nm
8H-a	0.1 per μm^2	21.5 ± 1.0 nm	N/A	15.8 ± 0.7 nm	<i>WD</i> 10.4 ± 0.5 nm
8H-b	0.1 per μm^2	21.5 ± 0.9 nm	N/A	18.2 ± 0.7 nm	<i>WD</i> 10.4 ± 0.5 nm
6H-a	2.1 per μm^2	16.2 ± 0.9 nm	N/A	11.3 ± 0.5 nm	<i>WD</i> 11.0 ± 0.8 nm
6H-b	0.6 per μm^2	16.1 ± 0.8 nm	N/A	9.3 ± 0.4 nm	<i>WD</i> 11.0 ± 0.7 nm
8H-hole-a	0.2 per μm^2	21.6 ± 1.0 nm	32.2 ± 0.9 nm	10.6 ± 0.4 nm	<i>D_x</i> 12.4 ± 1.3 nm <i>D_z</i> 17.9 ± 1.5 nm
8H-hole-b	0.5 per μm^2	21.5 ± 0.9 nm	32.2 ± 1.0 nm	10.8 ± 0.4 nm	<i>D_x</i> 9.3 ± 1.2 nm <i>D_z</i> 13.9 ± 1.5 nm
8H-hole-c	1.5 per μm^2	21.6 ± 0.9 nm	32.3 ± 1.0 nm	10.9 ± 0.3 nm	<i>D_x</i> 8.5 ± 1.1 nm <i>D_z</i> 11.7 ± 1.5 nm
8H-hole-d	2.4 per μm^2	21.5 ± 0.9 nm	32.3 ± 1.0 nm	10.8 ± 0.3 nm	<i>D_x</i> 7.9 ± 1.1 nm <i>D_z</i> 9.2 ± 1.5 nm
12H-grid	0.8 per μm^2	32.3 ± 0.9 nm	32.1 ± 0.9 nm	19.2 ± 0.7 nm	<i>WD_x</i> 13.2 ± 0.6 nm <i>WD_z</i> 12.9 ± 1.0 nm
12H-pillar	4.6 per μm^2	32.5 ± 1.6 nm	32.1 ± 1.9 nm	18.4 ± 0.8 nm	<i>WD_x</i> 16.5 ± 1.1 nm <i>WD_z</i> 19.2 ± 1.1 nm

(In the column of critical dimension, *WD* stands for width, and *D* stands for diameter.)

Supplementary Table 3. AFM/SEM measurement results of silicon patterns.

Silicon pattern	Defects rate	x-axis pitch	z-axis pitch	Height	Critical dimension	Aspect ratio
Si-12H-a	0.2 per μm^2	32.4 ± 0.6 nm	N/A	21.0 ± 0.6 nm	<i>WD</i> 10.9 ± 0.5 nm	~1.9
Si-12H-b	0 per μm^2	32.3 ± 0.4 nm	N/A	35.5 ± 0.7 nm	<i>WD</i> 12.2 ± 0.4 nm	~2.9
Si-10H-b	0 per μm^2	27.0 ± 0.4 nm	N/A	34.7 ± 0.8 nm	<i>WD</i> 11.0 ± 0.4 nm	~3.2
Si-8H-b 0H ₂	3.7 per μm^2	21.6 ± 0.7 nm	N/A	22.4 ± 0.8 nm	<i>WD</i> 11.4 ± 0.6 nm	~2.0
Si-8H-b 0.5H ₂	1.6 per μm^2	21.6 ± 0.6 nm	N/A	22.3 ± 0.7 nm	<i>WD</i> 12.3 ± 0.6 nm	~1.8
Si-8H-b 1.0H ₂	3.1 per μm^2	21.5 ± 0.6 nm	N/A	22.0 ± 0.7 nm	<i>WD</i> 13.6 ± 0.6 nm	~1.6
Si-6H-a	7.8 per μm^2	16.1 ± 0.7 nm	N/A	12.5 ± 0.8 nm	<i>WD</i> 9.8 ± 1.1 nm	~1.2
Si-6H-b	4.6 per μm^2	16.2 ± 0.6 nm	N/A	12.2 ± 0.6 nm	<i>WD</i> 9.3 ± 0.7 nm	~1.2
Si-8H-hole-a	0.9 per μm^2	21.6 ± 0.8 nm	32.2 ± 0.8 nm	12.4 ± 0.8 nm	<i>D_x</i> 12.8 ± 1.2 nm <i>D_z</i> 19.2 ± 1.5 nm	N/A
Si-8H-hole-b	1.2 per μm^2	21.5 ± 0.7 nm	32.2 ± 0.8 nm	12.5 ± 0.7 nm	<i>D_x</i> 10.7 ± 1.1 nm <i>D_z</i> 15.4 ± 1.4 nm	N/A
Si-8H-hole-c	2.1 per μm^2	21.6 ± 0.6 nm	32.3 ± 0.9 nm	12.2 ± 0.7 nm	<i>D_x</i> 8.3 ± 0.8 nm <i>D_z</i> 12.1 ± 1.3 nm	N/A
Si-8H-hole-d	5.4 per μm^2	21.7 ± 0.7 nm	32.2 ± 0.9 nm	12.8 ± 0.7 nm	<i>D_x</i> 7.2 ± 1.0 nm <i>D_z</i> 8.6 ± 1.4 nm	N/A
Si-12H-grid	8.1 per μm^2	32.3 ± 0.9 nm	32.0 ± 1.1 nm	19.6 ± 0.6 nm 17.5 ± 0.8 nm	<i>WD_x</i> 13.8 ± 0.8 nm <i>WD_z</i> 12.2 ± 0.9 nm	~1.4